RSC Advances

PAPER

View Article Online
View Journal | View Issue

Cite this: *RSC Adv.*, 2022, **12**, 27002

Ultra-efficient catalytic degradation of malachite green dye wastewater by $KMnO_4$-modified biochar (Mn/SRBC)†

Hao Zhu and Haiming Zou*

In this work, $KMnO_4$-modified biochar was prepared from spirulina residue as the research object. Herein, we report the synthesis, characterization, and catalytic degradation performance of $KMnO_4$-modified biochar, given that heterogeneous catalytic oxidation is an effective way to treat dye wastewater rapidly. The Mn/SRBC catalyst prepared by $KMnO_4$ modification was characterized by scanning electron microscopy, transmission electron microscopy, X-ray diffractometry, X-ray photoelectron spectroscopy, Fourier transform infrared spectroscopy, nitrogen adsorption–desorption and laser Raman spectroscopy. In addition, we compared the results with that of the unmodified SRBC. The results showed that the Mn/SRBC catalyst prepared by $KMnO_4$ modification had a rich pore structure, which provided sufficient contact area for the catalytic reaction. In the presence of H_2O_2, the catalyst could be used to catalyze the oxidative degradation of malachite green in aqueous solution with ultra-high efficiency. In the experiment, the initial pH values of the reaction system had a significant influence on the reaction rate. The removal effect of biochar on the malachite green was poor in an alkaline environment. Within a specific range, the removal rate of malachite green was proportional to the concentration of H_2O_2 in the reaction system. The degradation rate of malachite green dye at 8000 mg L^{-1} was about 99% in the presence of the catalyst over 5 mmol L^{-1} hydrogen peroxide for 30 min. These results show the potential application of algae residue biochar and carbon-based composite catalysts for degrading and removing dye wastewater.

Received 11th July 2022
Accepted 8th September 2022

DOI: 10.1039/d2ra04263k

rsc.li/rsc-advances

1. Introductions

Dyes and pigments are widely used in many industries for coloring products, such as textiles, leather, food, papermaking and pulp, printing, cosmetics, plastics, pharmaceuticals, and dye factories.[1] However, dyes and pigments may significantly affect the photosynthetic activity of aquatic organisms because they reduce the light penetration ability. Moreover, due to the presence of aromatic hydrocarbons, metals, and chlorides in dyes, they may also be toxic to some aquatic organisms and pose a continuous threat to the aquatic environment.[2] Malachite green (MG) is a veterinary antibiotic drug and a triphenylmethyl dye.[3] It is also widely used as a fungicide and parasiticide in aquaculture worldwide. However, it is highly toxic to mammalian cells and may have carcinogenic, teratogenic, and mutagenic effects.[4,5] It was reported that even low concentrations of malachite green discharged into receiving water will have a wide range of toxicological effects on various fish and some mammals. In addition, it causes harm to the liver, gills, kidney, intestine, gonad, and pituitary gonadotropin cells.[6] Therefore, the development of effective ways to deal with industrial wastewater has become an urgent task.

Simultaneously, spirulina produces many residues, which are mainly from the food processing and extraction of phycocyanin from spirulina. The deposition of phycocyanins extracted from spirulina usually accounts for 70% of microalgae biomass.[7] However, if these algal residues are not adequately handled, their entry in the environment from sewage discharge will lead to a series of environmental problems and cause wastage of resources. These algal residues contain abundant carbohydrates, proteins, or lipids.[8] Thus, some researchers have tried to recycle algal residues to produce alternative materials for wastewater treatment, such as biochar adsorbents.[9]

Over the years, there have been many reports in the literature on chemical coagulation, reverse osmosis, ion exchange, ozone, photooxidation, and other wastewater treatment methods.[10–13] However, these technologies have shortcomings such as incomplete removal, high cost, and side effects of additional waste, and the traditional water treatment methods have little impact on the degradation of refractory pollutants.[14] Recently, advanced oxidation processes (AOPs) with the advantages of high degradation efficiency, short reaction time, and nonselective degradation of various organic pollutants have been

Department of Resource and Environment, Anhui Science and Technology University, Fengyang 233100, People's Republic of China. E-mail: zouhm@ahstu.edu.cn

† Electronic supplementary information (ESI) available. See https://doi.org/10.1039/d2ra04263k

applied in dye wastewater treatment.[15–17] Advanced oxidation technology can generate potent oxidizing hydroxyl radicals ($^{\bullet}OH$) and sulfate radicals ($SO^{2-\bullet}$) through catalytic reactions under different conditions,[18] which has become an important direction of current research. The traditional Fenton reaction is widely used as advanced oxidation technology. However, it has some shortcomings,[19,20] as follows: (1) it easily produces iron sludge (Fe $(OH)_3$) precipitation, resulting in secondary pollution. (2) The pH range of the reaction is strict, where only acidic conditions are suitable. (3) Low utilization of H_2O_2 and high industrial costs. In addition to the traditional elements such as Fe,[21,22] Cu[23] and Mo,[24] Mn is also an active component of the commonly used H_2O_2 selective oxidation catalysts, which has attracted wide attention from researchers in recent years. Compared with the traditional Fenton reaction, this system has the advantages of a high utilization rate of H_2O_2, wide pH range, and no secondary pollutants, which is consistent with the concept of cleaner production.[25,26] At present, there are many studies on the degradation of organic contaminants by Mn/H_2O_2 systems.[27–29] However, there are few reports on the use of Mn and biochar composites as carbon-based catalysts.

Researchers found that biochar, as a solid material, exhibits the characteristics of loose and porous nature,[30] which makes its treatment effect more prominent and efficient. Especially in the adsorption of heavy metal–organic matter in the soil, biochar is not easily mineralized by microorganisms. It can promote the growth of microorganisms in the ground. In recent years, biochar has attracted much attention due to its unique physical and chemical properties. However, the number of oxygen-containing functional groups and the specific surface area of biochar produced by simple thermal and chemical reactions are low.[31,32] In the preparation process, the introduction of other compounds to modify biochar can increase its surface area and functional groups and improve its adsorption and catalytic performance.[33,34] Potassium permanganate ($KMnO_4$) as a strong oxidant decomposition can generate MnO_x (ref. 35 and 36) and has the advantages of being safe and nontoxic. At present, as a modified reagent, it is also widely used in experimental and industrial removal applications and has achieved an excellent modification effect.[37] However, the use of algae residue as biomass raw material to prepare biochar as a catalyst for advanced oxidation technology has rarely been reported. In addition, the research on metal oxide-modified biochar as a catalyst is not thorough.

In this study, Mn/SRBC ($KMnO_4$-modified spirulina residue biochar) catalysts were prepared *via* the chemical coprecipitation pyrolysis of $KMnO_4$ and spirulina residue biochar, improving the dispersion of the MnO_x particles and enhancing their performance. The treatment of malachite green by Fenton-like oxidation improves the application scope of Fenton oxidation, reduces the cost of secondary treatment, and improves the effect of advanced oxidation technology on malachite green. High-resolution transmission electron microscopy (TEM), scanning electron microscopy (SEM), X-ray diffraction (XRD), Fourier transform infrared spectroscopy (FTIR), and laser Raman spectroscopy (Raman) were used to characterize the Mn/SRBC catalysts. The main structure of malachite green is triphenylmethane, which has representatives of some dyes. Therefore, in this experiment, we selected malachite green dye-simulated printing and dyeing wastewater as the treatment object. By detecting the absorbance of the solution at each stage of oscillation, this experiment was performed to study the effects of the initial pH value of the reaction system, the dosage of the Mn/SRBC catalyst, the concentration of H_2O_2, and the initial concentration of malachite green on the degradation of malachite green dye by the Mn/SRBC catalysts. The results revealed the specific effects of the Mn/SRBC catalysts on removing malachite green dye wastewater. In addition, this study provides the theoretical basis for developing valuable algal residue biochar and the effective degradation and practical application of malachite green dye wastewater.

2. Materials and methods

2.1. Reagents and materials

Malachite green ($C_{23}H_{25}ClN_2$, MG), sodium hydroxide (NaOH), hydrochloric acid (HCl), potassium bromide (KBr, FW), and anhydrous ethanol (C_2H_6O, FW) were all analytically pure. Deionized water was made in the laboratory.

2.2. Preparation of Mn/SRBC catalysts

The Mn/SRBC catalyst was prepared *via* chemical coprecipitation pyrolysis. The preparation process was as follows: spirulina residue was washed to neutral with deionized water and transferred to a constant temperature oven for drying at 75 °C. Then, $KMnO_4$ was added to the algal residue according to the proportion of 0.005 mol modified compound per gram of biomass. In the experiments, ionic water was added to make it immersed. At room temperature, it was oscillated for 24 h on a constant temperature oscillator at a speed of 150 r per min and the material obtained after oscillation dried to a stable weight in an oven. The obtained dry solids were broken into pieces and ground through a 50 mesh screen. Then, the sample was placed in a crucible, wrapped with tin paper to isolate the air, and placed in a muffle furnace and heated to 500 °C at a heating rate of 20 °C min^{-1} for 3 h. After pyrolysis, the obtained catalyst was sealed for preservation.

2.3. Characterization techniques

The Mn/SRBC catalysts were characterized by high-resolution transmission electron microscopy (TEM, JEM-2100F, Japan Electronics Corporation, Japan) and scanning electron microscopy (SEM, EVO-18, Carl Zeiss, Germany). The crystal structure characteristics of the Mn/SRBC catalysts were analyzed and tested using an X-ray diffractometer (XRD, XD-3, PXG, China) in the test range of 2θ = 10–60° at the scanning speed of 5° per min, with the current of 24 mA and the voltage of 36 kV. The material composition and the atomic valence state of the Mn/SRBC catalyst were analyzed by X-ray photoelectron spectroscopy (XPS, EscaLab 250Xi, Thermo, America). The surface functional groups of the Mn/SRBC catalysts were characterized by Fourier transform infrared spectroscopy (FTIR, FTIR-850, Tianjin Gangdong Science and Technology, China). The

catalysts were prepared using the KBr tableting method to determine the their surface functional groups in wavenumber range of 4000–500 cm^{-1} at the resolution of 2 cm^{-1} and number of scans of 32. The molecular structure of the Mn/SRBC catalysts was characterized by laser Raman spectroscopy (Raman Spectra, XploRA PLUS, HORIBA Group, Japan) at the laser wavelength of 750 nm and wavenumber range of 500–3000 cm^{-1}. An automatic specific surface area and porosity analyzer (BET, ASAP 2460, Micromeritics, America) were used to determine the surface area, pore size, and pore volume of the samples. Firstly, a certain amount of sample to be tested was degassed under vacuum at 200 °C for a while. Nitrogen adsorption and desorption were measured using an automatic specific surface area and porosity analyzer at 77 K. The surface area was calculated using the Brunauer–Emmett–Teller (BET) method and the pore-size distribution calculated using the Barrett–Joyner–Halenda (BJH) method.

2.4. Catalytic degradation experiment

2.4.1. Effect of pH value. Briefly, 5 mmol L^{-1} H_2O_2 was added to a malachite green solution (8000 mg L^{-1}) and the pH was adjusted to 1.0, 3.0, 5.0, 7.0 and 9.0 with 1 mol L^{-1} NaOH and HCl, respectively. The Mn/SRBC catalyst prepared by adding 2.0 g L^{-1} Mn/SRBC was placed in a 250 r per min constant temperature oscillator, and the catalyst was added simultaneously. Then 5 mL solution was sampled at 0, 2, 5, 10, 20, 30, 60, and 90 min, and the sample was filtered using a 0.45 μm polyethersulfone (PES) filter membrane. The absorbance of malachite green was determined at 617 nm.[3]

2.4.2. Effect of catalyst dosage. Briefly, 5 mmol L^{-1} H_2O_2 was added to a malachite green solution (8000 mg L^{-1}), and the pH was adjusted to 3.0 with 1 mol L^{-1} NaOH or HCl. The Mn/SRBC catalysts prepared at a dose of 1.0, 1.5, 2.0, and 2.5 g L^{-1} were added to the reaction system and placed in a 250 r per min thermostatic oscillator. The catalysts were added, and the time was counted. Then 5 mL solution was sampled at 0, 2, 5, 10, 20, 30, 60, and 90 min, and the sample was filtered using a 0.45 μm polyethersulfone (PES) filter membrane. The absorbance of malachite green was determined at 617 nm.

2.4.3. Effect of H_2O_2 concentration. Briefly, 2, 5, 10, and 15 mmol L^{-1} H_2O_2 was added to a malachite green solution (8000 mg L^{-1}), and then the pH was adjusted to 3.0 with 1 mol L^{-1} NaOH or HCl. The Mn/SRBC catalyst prepared by adding 2.0 g L^{-1} Mn/SRBC was placed in a 250 r per min constant temperature oscillator, and the catalyst was added simultaneously. Then 5 mL solution was sampled at 0, 2, 5, 10, 20, 30, 60, and 90 min, and the sample was filtered using a 0.45 μm polyethersulfone (PES) filter membrane. The absorbance of malachite green was determined at 617 nm.

2.4.4. Effect of initial concentration of malachite green. Briefly, 5 mmol L^{-1} H_2O_2 was added to 4000 mg L^{-1}, 6000 mg L^{-1}, 8000 mg L^{-1}, and 10 000 mg L^{-1} malachite green solution, and then the pH was adjusted to 3.0 with 1 mol L^{-1} NaOH or HCl. The Mn/SRBC catalyst prepared by adding 2.0 g L^{-1} Mn/SRBC was placed in a 250 r per min constant temperature oscillator, and the catalyst was added simultaneously. Then 5 mL solution was sampled at 0, 2, 5, 10, 20, 30, 60, and 90 min, and the sample was filtered using a 0.45 μm polyethersulfone (PES) filter membrane. The absorbance of malachite green was determined at 617 nm.

2.5. Data processing and analysis

The degradation effect of malachite green by catalytic oxidation is expressed by the removal rate, and the calculation formula is as follows:

$$\eta = 1 - C_e/C_0 \quad (1)$$

where C_0 is the concentration of malachite green at the initial time in mg L^{-1}. C_e is the concentration of malachite green at equilibrium time in mg L^{-1} η is the removal rate in %.

Each treatment was repeated three times independently, with the average value as the test result, and the data were analyzed using SPSS 25.0, and the OriginPro 18 drawing software.

3. Results and discussion

3.1. SEM and TEM studies

The SEM and TEM micrographs of the SRBC and Mn/SRBC biochar samples pre-and post $KMnO_4$ modification are shown in Fig. 1. SEM was employed to directly observe the surface differences in the different samples. As shown in Fig. 1(a), SRBC biochar is granular and its pore structure was not developed. In contrast, Fig. 1(b) shows that the surface roughness and porosity of the Mn/SRBC biochar increased significantly upon $KMnO_4$ modification, with the appearance of many flocculent particles. The increase in roughness and porosity helps to provide more contact area for the catalytic reaction, thereby improving the removal rate. As shown in Fig. 1(c) and (d), the SRBC and Mn/SRBC biochar have pronounced graphite-like lamellar structures with a thin biochar layer, respectively. After $KMnO_4$ modification, the Mn/SRBC biochar was doped with many aggregate particles (see Fig. 1(d)), and thus its composition and morphology needed further determination and analysis.

3.2. XRD studies

XRD analysis is an essential means to study the internal crystalline structure of materials.[38] To further analyze the morphology of the agglomerate particles on the algal residue biochar, the crystal structure characteristics of the SRBC and Mn/SRBC biochar samples pre-and post $KMnO_4$ modification were analyzed by X-ray diffraction. The analysis results are shown in Fig. 2. A wide diffraction peak appeared at $2\theta = 10–30°$ in the spectra of SRBC and Mn/SRBC, indicating that the organic matter in SRBC and Mn/SRBC was highly carbonized to form amorphous carbon.[39,40] New pronounced diffraction peaks appeared at the 2θ values of 34.9°, 40.5° and 58.7° for Mn/SRBC, among which the peak at $2\theta = 40.5°$ was the strongest. These characteristic peaks are consistent with the standard diffraction card (PDF 00-007-0230, MnO_2), which proved that Mn/SRBC contained MnO_x. In the dry pyrolysis of spirulina residue,

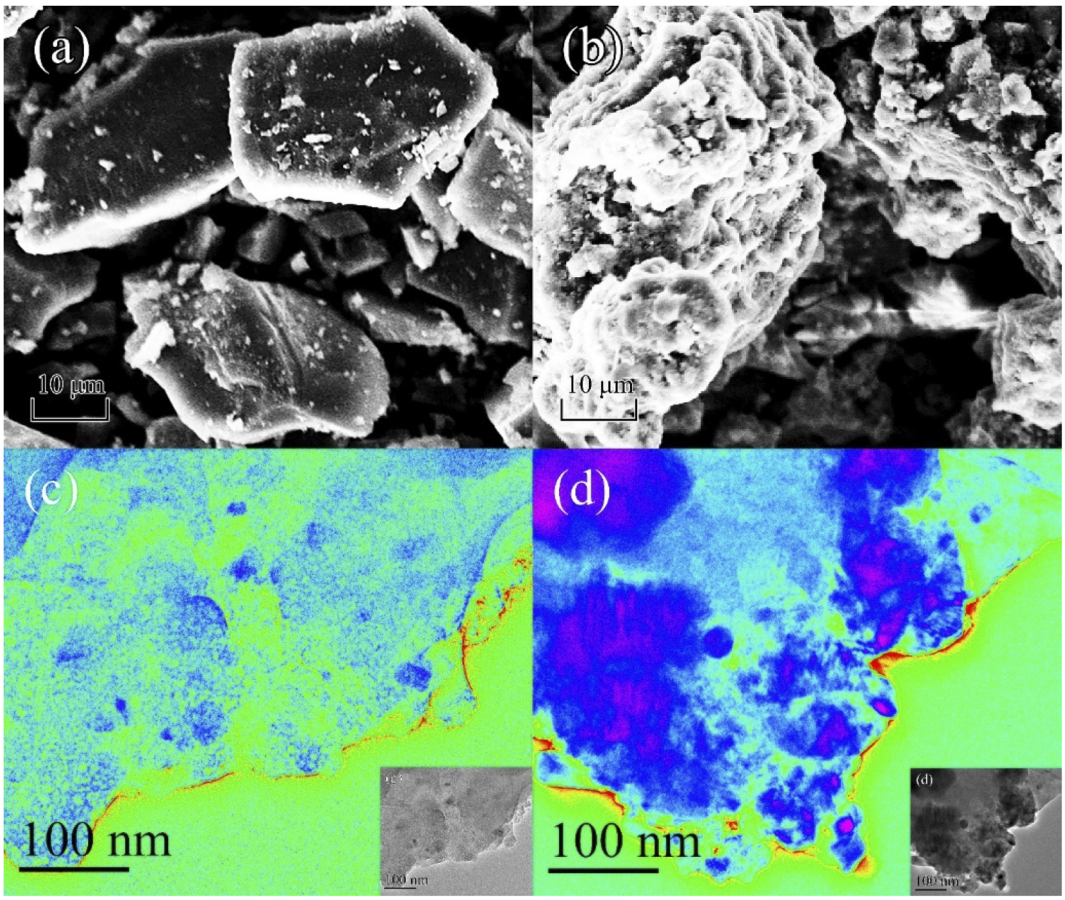

Fig. 1 SEM micrographs of the different samples for (a) SRBC and (b) Mn/SRBC. TEM micrographs of the different samples for (c) SRBC and (d) Mn/SRBC.

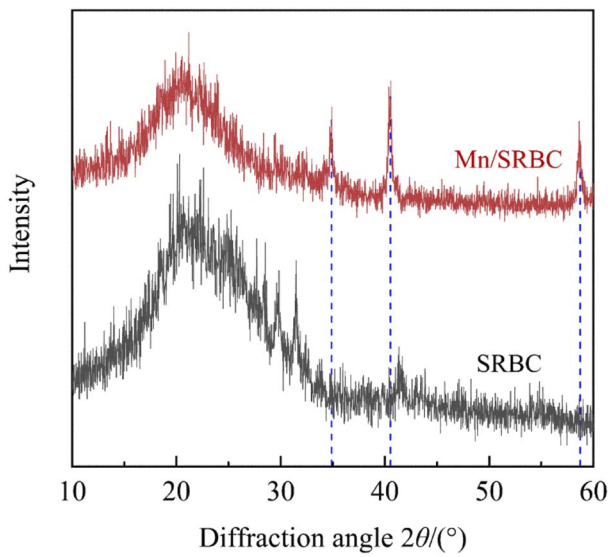

Fig. 2 XRD spectra of Mn/SRBC and SRBC.

$KMnO_4$ with strong oxidation will react with carbon to form aggregates of manganese oxides, which is consistent with the TEM analysis results.

3.3. XPS studies

The XPS spectra of SRBC and Mn/SRBC are shown in Fig. 3. XPS analysis is an effective measure for understanding the oxidation state of transition metal ions and the relative composition of composite materials.[41]

Fig. 3(a) and (b) show the XPS wide-mode spectra of SRBC and Mn/SRBC, respectively. This figure shows that the Mn element was successfully loaded on Mn/SRBC prepared by modification, which is consistent with the XRD analysis results. Fig. 3(c) shows the Mn 2p XPS spectra of SRBC and Mn/SRBC. The electron binding energy peaks of MnO_x in Mn/SRBC can be observed at 642.3 eV (Mn $2p_{3/2}$) and 653.7 eV (Mn $2p_{1/2}$), which further indicates that the Mn element in Mn/SRBC exists in the form of MnO_x.[42,43] To further confirm the valence composition of the Mn element in Mn/SRBC, the Mn 3s core level spectrum of Mn/SRBC was measured, as shown in Fig. 3(d). The energy separation between the two peaks of Mn 3s is related to the mean manganese oxidation state. Given that a lower valence implies more electrons in the 3d orbital, more interaction can occur upon photoelectron ejection. Consequently, the energy separation between the two components of the Mn 3s multiplet will increase. The inverse trend will be observed when the manganese valency increases.[44,45] Thus, the

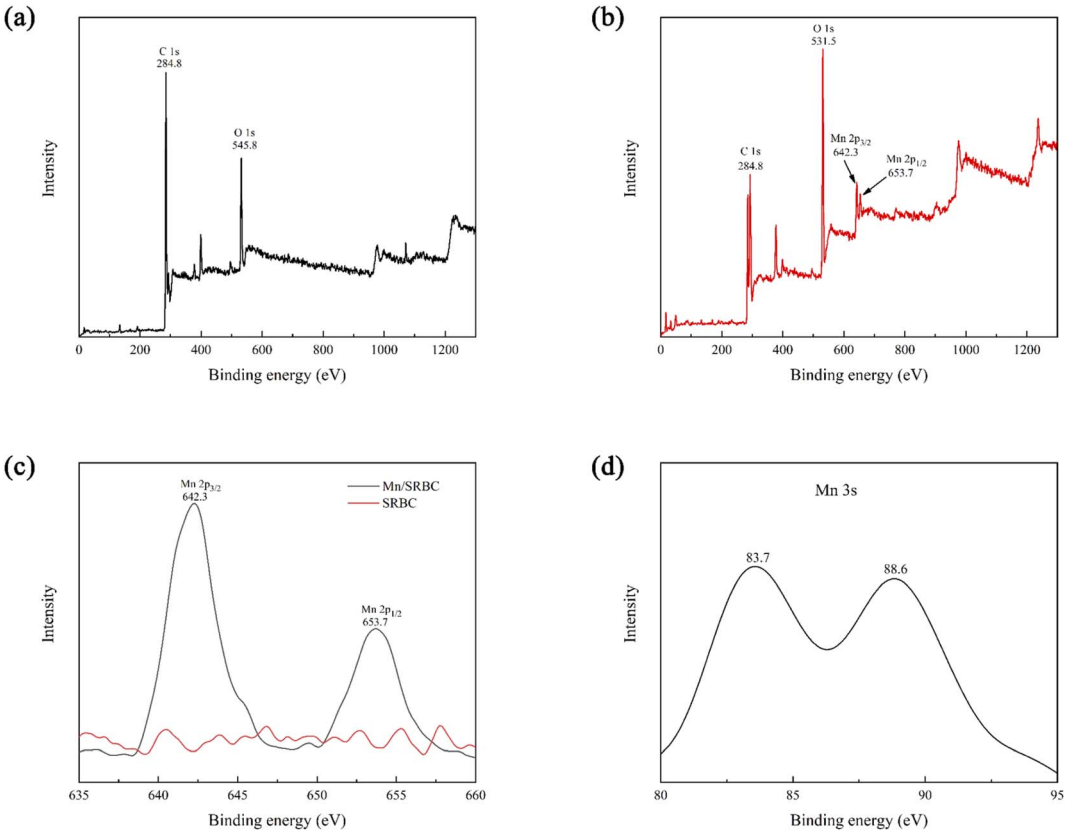

Fig. 3 XPS spectra of SRBC and Mn/SRBC. Wide-mode spectra of (a) SRBC and (b) Mn/SRBC. (c) Mn 2p XPS spectra of SRBC and Mn/SRBC and (d) Mn 3s spectra of Mn/SRBC.

result can be employed to determine the oxidation state of Mn from the peak separation of couples of the Mn 3s spectrum. Mn with the +4 oxidation state shows a peak separation of 4.7–4.8 eV in the 3s level. In the catalyst Mn/SRBC, the above-mentioned peak split was determined to be 4.9 eV (shown in Fig. 3(d)), implying that Mn exists in the +3 and +4 oxidation states.[46]

3.4. FTIR studies

The FTIR results for the SRBC and Mn/SRBC biochar samples before and after $KMnO_4$ modification are shown in Fig. 4. The modification had an important influence on the structure and properties of the biochar. FTIR is one of the effective means to measure the functional groups in biochar.[47] The absorption peaks of the SRBC and Mn/SRBC biochar before and after $KMnO_4$ modification are similar in the high wavenumber region above 1500 cm^{-1} and near 1000 cm^{-1}. Among the peaks, the broad and strong peak centered at 3457 cm^{-1} indicates the presence of O–H. The absorption peak at 2992 cm^{-1} corresponds to the stretching vibration peak of aliphatic C–H, reflecting the presence of aliphatic $-CH_3$ or $-CH_2$ groups.[48] The two peaks at 1635 cm^{-1} and 1060 cm^{-1} are attributed to the stretching vibration of the aromatic ring C=C and the stretching vibration of C–H, respectively, indicating that these biochars generated carbon with an aromatic structure.[49,50] Fourier transform infrared spectroscopy analysis showed that the composition of SRBC and Mn/SRBC biochar before and after $KMnO_4$ modification was similar, but the number of functional groups was significantly different, which led to the difference in the intensity of their absorption peaks. As shown in Fig. 4, the two weak peaks at 848 cm^{-1} and 615 cm^{-1} are ascribed to MnO_x,[51] which further prove that MnO_x was formed on the surface of the modified hydrothermal carbon.

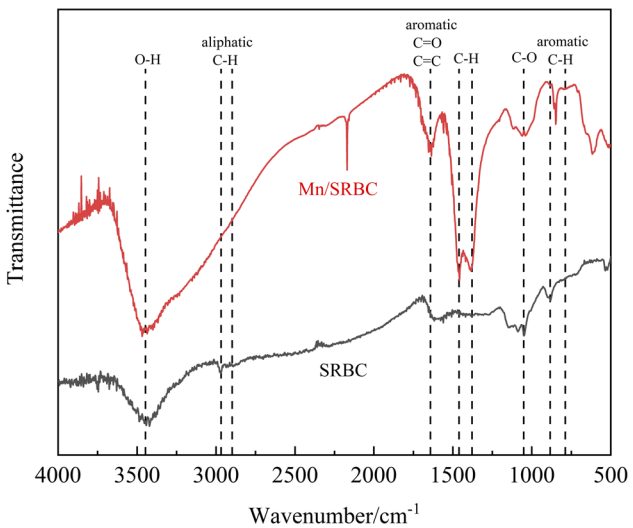

Fig. 4 FTIR spectra of Mn/SRBC and SRBC.

3.5. Raman studies

Raman spectroscopy is an effective method for the rapid evaluation of the properties and molecular structure analysis of biochar.[52] The Raman spectra of SRBC and Mn/SRBC biochar modified by $KMnO_4$ are shown in Fig. 5. Generally, carbon materials have two characteristic bands, *i.e.*, D and G bands. The D band originates from the sp^3 hybridization of disordered carbon or defective graphite structures or carbon atom in the material. In contrast, the G band represents the in-plane stretching vibration of sp^2 hybridization.[53] The ratio of these two bands (I_D/I_G) is an indicator of graphitization.[54] The lower I_D/I_G, the higher the degree of graphitization.[55] The presence of a D band in the spectra of SRBC and Mn/SRBC indicates the presence of defects in the internal structure of biochar, thus confirming the existence of sp^3 structure in the biochar samples. The G band of SRBC and Mn/SRBC indicates that sp^2 hybridization exists in their structure. The peak area ratio (I_D/I_G) of the D band (1350 cm^{-1}) and the G band (1580 cm^{-1}) of SRBC and Mn/SRBC biochar modified by $KMnO_4$ did not change significantly (see Fig. 5). At the same temperature, through pyrolysis, lignin, cellulose, and other oxygen-containing functional groups in the biochar gradually decomposed into stable aromatic carbon structures.[56] However, the use of $KMnO_4$ to modify biochar did not change the pyrolysis temperature of biochar; accordingly, the degree of carbonization of biochar was the same, and thus I_D/I_G ratio was the same.

3.6. BET surface area studies

BET is usually used to reflect the number of reaction sites (adsorption or catalysis) on the sample surface. The nitrogen adsorption–desorption isotherms of Mn/SRBC are shown in Fig. 6. The specific surface area of Mn/SRBC was listed in Table 1. This curve attribute IV isotherm (based on IUPAC) indicates an obvious hysteresis loop in the adsorption/desorption process and has a typical mesoporous porous material type. The specific surface area of SRBC is small, and the instrument cannot be detected, which is consistent with the analysis results of SEM. The coincidence of desorption isotherms and adsorption isotherms indicated that there were different pore structures in Mn/SRBC. The adsorption/desorption isotherms were separated at a high relative pressure ($P/P_0 > 0.75$), indicating that the prepared Mn/SRBC had more mesopores and macropores. Which can know that the modified Mn/SRBC has a higher specific surface area and porosity than SRBC, which provides more reaction sites for catalytic reaction and is more conducive to the catalytic reaction.

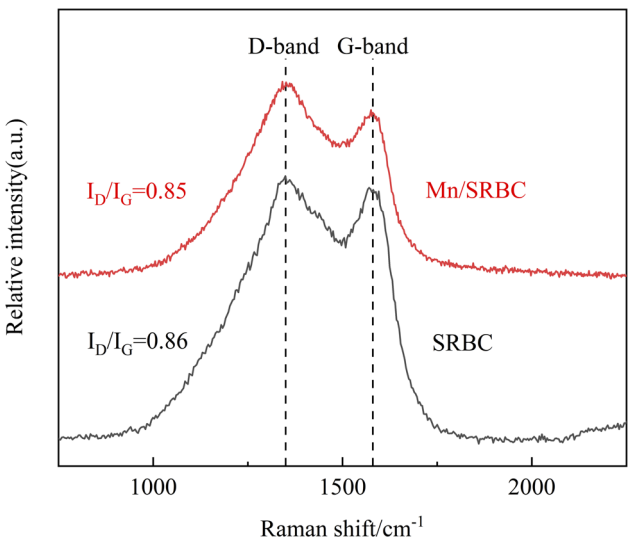

Fig. 5 Raman spectra of Mn/SRBC and SRBC.

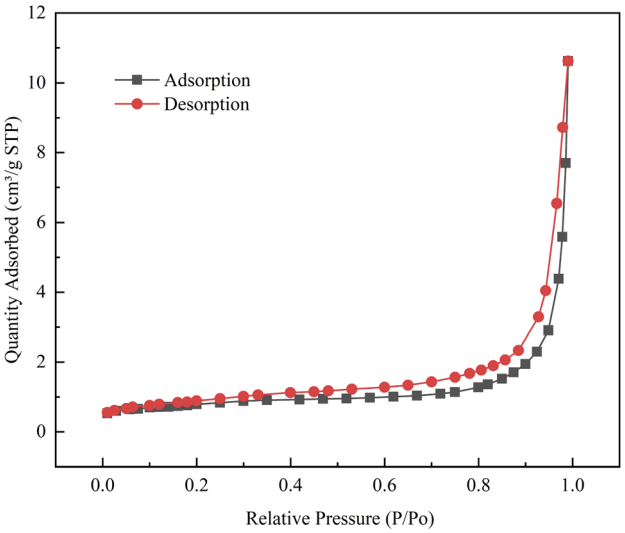

Fig. 6 Nitrogen adsorption–desorption isotherm of Mn/SRBC.

Table 1 Surface area and pore structure parameters of Mn/SRBC

Material	Surface area ($m^2\ g^{-1}$)	Average pore diameter (nm)	Pore volume $P/P_0 = 0.991$ ($cm^3\ g^{-1}$)
Mn/SRBC	2.766	22.596	0.016

3.7. Effect of initial pH

In the catalytic degradation of malachite green using the potassium permanganate-modified biochar, the initial pH value of the reaction system will have a particular impact on the experimental results. Thus, an experiment was performed to explore the effect of Mn/SRBC catalytic oxidation on the degradation of malachite green dye by changing the initial pH value of the reaction system. At room temperature, the pH value of the reaction system was adjusted to 1.0, 3.0, 5.0, 7.0, and 9.0, and 2.0 g L^{-1} catalyst Mn/SRBC was added. Simultaneously, the reaction began. The absorbance of malachite green was measured at a specific time in the experimental design. The removal rate of malachite green dye varied with time, as shown in Fig. 7(a). The results show that the change in the initial pH value of the reaction system has a significant impact on the catalytic degradation of malachite green. With an increase in pH value, the removal time gradually increased. When pH = 1.0, the removal rate was almost zero. When pH = 3.0, the removal

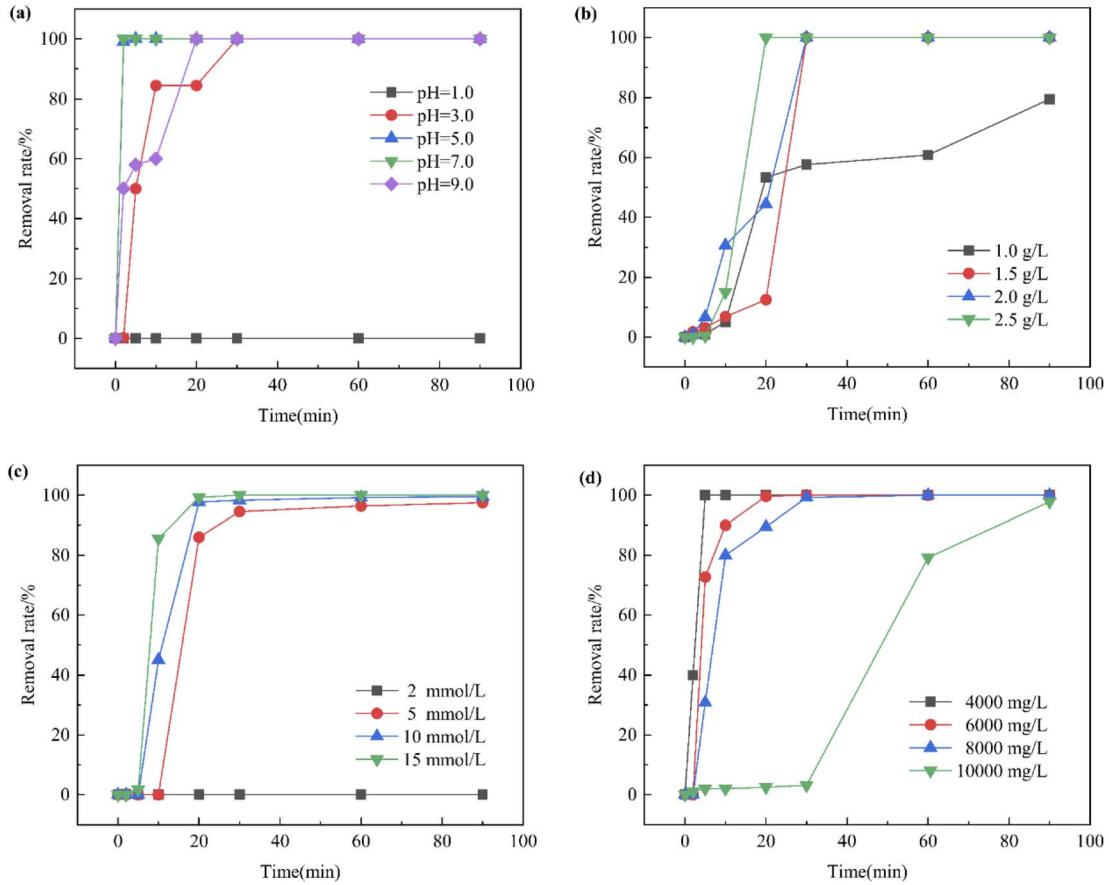

Fig. 7 Effects of different factors including (a) initial pH; (b) catalyst dosage; (c) H_2O_2 concentration; and (d) initial concentration of malachite green.

rate increased rapidly in 0–10 min, which tended to be stable in 10–20 min, and the removal rate increased to 100% within 30 min, and the effect changed significantly. When the pH was 5.0 and 7.0, the remove rate increased rapidly and tended to 99% within 1 min. When the pH was 9.0, the removal rate was relatively slow in 2–10 min, and the reaction accelerated the remove ratal in 10–20 min. When the reaction proceeded to 20 min, the removal rate tended to 100%. At higher pH, Mn is known to interact with OH^- to form manganese hydrous oxides (due to the oxo-metal chelation),[41] which causes malachite green degradation at a slower rate.

3.8. Effect of catalyst dosage

In the process of malachite green degradation by the potassium permanganate-modified biochar, the dosage of catalysts will have a particular influence on the experimental results. In this experiment, we explored the effect of Mn/SRBC catalytic oxidation on the degradation of malachite green dye by changing the dosage of Mn/SRBC biochar. At room temperature, when the pH value of the reaction system was 3.0, 1.0, 1.5, 2.0, and 2.5 g L^{-1} Mn/SRBC catalyst was added to the reaction system containing 5 mmol L^{-1} H_2O_2 solution. Simultaneously, the reaction began. The absorbance of malachite green was measured at a specific time in the experimental design. The removal rate of malachite green dye varied with time, as shown in Fig. 7(b). The results show that the addition of different amounts of catalyst to the reaction system had a significant impact on the catalytic oxidation of malachite green by Mn/SRBC, and the removal efficiency of malachite green is proportional to the amount of catalyst added. When the catalyst dosage was 1.0 g L^{-1}, the removal efficiency within 90 min was only 79.5%. As shown in Fig. 7(b), when the reaction proceeded to 20 min, the removal rate of 1.5 g L^{-1} Mn/SRBC catalyst was 12.5%, that for 2.0 g L^{-1} catalyst was 44.4%, while that for 2.5 g L^{-1} catalyst was 100%. With an increase in the amount of Mn/SRBC catalyst, the number of reaction sites increased, and more oxidizing species such as hydroxyl radicals are generated on the catalyst surface, and thus the better the catalytic degradation effect of malachite green dye. In addition, with an increase in catalyst dosage, the adsorption of malachite green on the catalyst itself increased. Therefore, 2.5 g L^{-1} Mn/SRBC catalyst had the best effect on malachite green treatment.

3.9. Effect of H_2O_2 concentration

In the catalytic degradation of malachite green by the potassium permanganate-modified biochar, the concentration of H_2O_2 will have a particular impact on the experimental results. Thus, in this experiment, we explored the effect of Mn/SRBC catalytic oxidation on the degradation of malachite green dye by changing

the concentration of H_2O_2. At room temperature, the initial pH of the reaction system was 3.0, and 2, 5, 10, and 15 mmol L^{-1} H_2O_2 was added to the reaction system, and then 2.0 g L^{-1} of modified biochar was added. Simultaneously, the reaction began. The absorbance of malachite green was measured at a specific time in the experimental design. The removal rate of malachite green dye changed with time, as shown in Fig. 7(c). The results show that different H_2O_2 concentrations in the reaction system had a significant impact on the catalytic oxidation of malachite green by the Mn/SRBC catalyst. With an increase in the H_2O_2 concentration, the removal rate of malachite green by the biochar gradually increased. When the concentration of H_2O_2 was 2 mmol L^{-1}, the removal effect of Mn/SRBC on malachite green was not pronounced. When the concentration of H_2O_2 is high, due to its strong oxidation, the reaction with Mn/SRBC catalyst will be more rapid and violent, accelerating the decomposition of H_2O_2 itself into O_2 and H_2O, and thus the removal rate of malachite dye does not improve much.[57] In summary, this study indicates that 5 mmol L^{-1} of H_2O_2 should be added to the reaction system.

3.10. Effect of initial concentration of malachite green

In the process of catalytic degradation of malachite green by Mn/SRBC, the initial concentration of malachite green will have a particular impact on the experimental results. Thus, in this experiment, we explored the effect of Mn/SRBC catalytic oxidation on the degradation of malachite green dye by changing the initial concentration of malachite green. In this experiment, the malachite green solution at room temperature had a concentration of 4000, 6000, 8000, and 10 000 mg L^{-1}, with the condition of pH value of 3.0, 2.0 g L^{-1} Mn/SRBC catalyst and 30% H_2O_2 solution with a concentration of 5 mmol L^{-1} added to the reaction system, respectively. Simultaneously, the reaction began. The absorbance of malachite green was measured at a specific time in the experimental design. The removal rate of malachite green dye changed with time, as shown in Fig. 7(d). The results show that with an increase in the initial concentration, the removal efficiency of malachite green by Mn/SRBC Fenton-like treatment decreased gradually, indicating that the initial concentration of malachite green is a prominent factor for the study of the treatment effect of malachite green. When the initial concentrations were 6000, 8000, and 10 000 mg L^{-1}, the treatment effect of Mn/SRBC on malachite green was not apparent in the first 2 min. However, with a change in time, the removal rate of malachite green by biochar treatment increased. Saha S, *et al.*[46] used 0.5 g L^{-1} MnO_2 to catalyze the degradation of 50 mg L^{-1} malachite green. The decolorization rate reached 99% and the mineralization rate reached 44% in 120 min, which were lower than the effect of Mn/SRBC on the catalytic degradation of malachite green in this study.

3.11. Recovery and reuse of Mn/SRBC catalysts

The Mn/SRBC catalysts were recovered after the degradation of malachite green and reused. The material was collected by centrifugation, and then dried in an oven at 90 °C for 12 h. To examine the reusability of the catalyst, the condition of pH value of 3.0 and 2.0 g L^{-1} Mn/SRBC catalyst and 30% H_2O_2 solution with a concentration of 5 mmol L^{-1} were added to the reaction system. The degradation of malachite green was monitored at a regular interval for three cycles of operations (see Fig. 8). It was observed that while malachite green was degraded up to 100% with the fresh Mn/SRBC catalyst within 90 min of reaction, 82.1% and 62.3% degradation could be achieved in the 2nd and 3rd cycles, respectively. This is due to the inactivation of the Mn/SRBC catalyst surface during the oxidation process. Besides, the material could be used further with a lower efficiency.

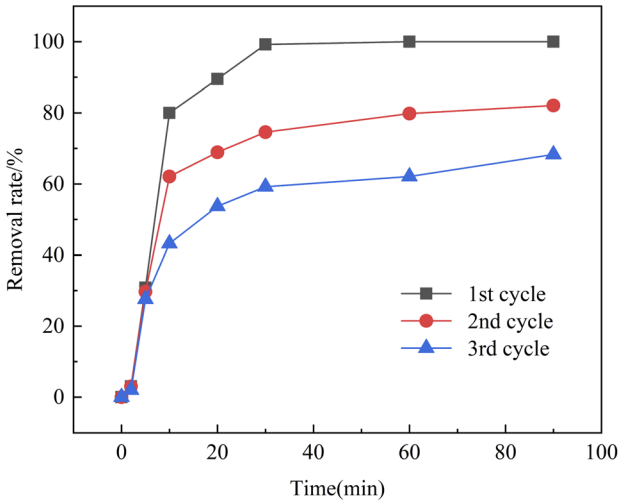

Fig. 8 Degradation of malachite green by Mn/SRBC catalyst.

4. Conclusions

A novel Mn-biochar (Mn/SRBC) carbon-based catalyst was successfully synthesized by $KMnO_4$ modification. The catalyst was characterized by SEM, TEM, XRD, FTIR, and Raman spectroscopy. The TEM and XRD analysis showed that manganese oxide MnO_x was successfully synthesized in the pyrolysis process of algae residue biochar modified by $KMnO_4$ *via* the chemical coprecipitation method. In the presence of H_2O_2, the catalyst could be used to catalyze the oxidative degradation of malachite green in aqueous solution with ultra-high efficiency. The degradation rate of malachite green dye at a concentration of 8000 mg L^{-1} was about 99% in the presence of the catalyst with 5 mmol L^{-1} hydrogen peroxide for 30 min. Moreover, given that the catalyst was heterogeneous and Fenton like, they could be easily separated from the reaction mixture. Therefore, according to the results from this study, it can be concluded that the Mn/SRBC catalyst has excellent catalytic performance and low cost. The raw material was obtained from spirulina residue, reflecting the ecological and environmental protection concept of waste treatment. The Mn/SRBC catalyst is a beneficial new catalyst for removing organic dye-contaminated wastewater.

Data availability

The data used to support the findings of this study are available from the corresponding author upon request.

Conflicts of interest

The authors declare that there is no conflict of interest regarding the publication of this paper.

Acknowledgements

This research is supported by the grant 2008085ME169 from Natural Science Foundation of Anhui Province, China and the grant 202103b06020018 from Major science and technology projects of Anhui Province, China.

References

1 N. B. Swan and M. A. A. Zaini, Adsorption of Malachite Green and Congo Red Dyes from Water: Recent Progress and Future Outlook, *Ecol. Chem. Eng. S*, 2019, **26**(1), 119–132.
2 A. Ausavasukhi, C. Kampoosaen and O. Kengnok, Adsorption characteristics of Congo red on carbonized leonardite, *J. Cleaner Prod.*, 2016, **134**, 506–514.
3 A. S. Y. Ting and J. E. Chin, Biogenic Synthesis of Iron Nanoparticles from Apple Peel Extracts for Decolorization of Malachite Green Dye, *Water, Air, Soil Pollut.*, 2020, **231**(6), 1–10.
4 L. Zeng, L. Xiao, Y. Long, *et al.*, Trichloroacetic acid-modulated synthesis of polyoxometalate@UiO-66 for selective adsorption of cationic dyes, *J. Colloid Interface Sci.*, 2018, **516**, 274–283.
5 Y. Yang, G. Wang, B. Wang, *et al.*, Decolorization of Malachite Green by a Newly Isolated *Penicillium* sp. YW 01 and Optimization of Decolorization Parameters, *Environ. Eng. Sci.*, 2011, **28**(8), 555–562.
6 S. Srivastava, R. Sinha and D. Roy, Toxicological effects of malachite green, *Aquat. Toxicol.*, 2004, **66**(3), 319–329.
7 Q. Yan, M. Zhao, H. Miao, *et al.*, Coupling of the hydrogen and polyhydroxyalkanoates (PHA) production through anaerobic digestion from Taihu blue algae, *Bioresour. Technol.*, 2010, **101**(12), 4508–4512.
8 F. Deniz and R. A. Kepekci, Equilibrium and kinetic studies of azo dye molecules biosorption on phycocyanin-extracted residual biomass of microalga Spirulina *platensis*, *Desalin. Water Treat.*, 2015, **57**(26), 12257–12263.
9 H. Zhang, F. Zhang and Q. Huang, Highly effective removal of malachite green from aqueous solution by hydrochar derived from phycocyanin-extracted algal bloom residues through hydrothermal carbonization, *RSC Adv.*, 2017, **7**(10), 5790–5799.
10 R. P. F. Melo, S. K. S. Carmo, E. L. B. Barros, *et al.*, Removal of Disperse Blue 56 from synthetic textile effluent using ionic flocculation, *Water Sci. Technol.*, 2021, **83**(11), 2714–2723.
11 K. K. Shimabuku, J. P. Kearns, J. E. Martinez, *et al.*, Biochar sorbents for sulfamethoxazole removal from surface water, stormwater, and wastewater effluent, *Water Res.*, 2016, **96**, 236–245.
12 K. Rajala, O. Gronfors, M. Hesampour, *et al.*, Removal of microplastics from secondary wastewater treatment plant effluent by coagulation/flocculation with iron, aluminum and polyamine-based chemicals, *Water Res.*, 2020, **183**, 116045.
13 I. Schneider, A. Abbas, A. Bollmann, *et al.*, Post-treatment of ozonated wastewater with activated carbon and biofiltration compared to membrane bioreactors: Toxicity removal *in vitro* and in Potamopyrgus antipodarum, *Water Res.*, 2020, **185**, 116104.
14 F. Li, Q. Xia, Y. Gao, *et al.*, Anaerobic biodegradation and decolorization of a refractory acid dye by a forward osmosis membrane bioreactor, *Environ. Sci.: Water Res. Technol.*, 2018, **4**(2), 272–280.
15 S. Cai, S. Zhang, C. Gao, *et al.*, Degradation of fluorescent dye-Solvent Green 7 (HPTS) in wastewater by advanced oxidation process, *Water Sci. Technol.*, 2020, **82**(11), 2525–2535.
16 S. Hashemian, Fenton-Like Oxidation of Malachite Green Solutions: Kinetic and Thermodynamic Study, *J. Chem.*, 2013, **2013**, 1–7.
17 P. Dinh Du, H. Thanh Danh, P. Ngoc Hoai, *et al.*, Heterogeneous UV/Fenton-Like Degradation of Methyl Orange Using Iron Terephthalate MIL-53 Catalyst, *J. Chem.*, 2020, **2020**, 1–13.
18 A. M. Wang, C. H. Wu and E. H. Huang, Removal of sulfamethizole from aqueous solution using advanced oxidation processes: effects of pH and salinity, *Water Sci. Technol.*, 2020, **82**(11), 2425–2431.
19 A. Mirzaei, Z. Chen, F. Haghighat, *et al.*, Removal of pharmaceuticals from water by homo/heterogonous Fenton-type processes – A review, *Chemosphere*, 2017, **174**, 665–688.
20 H. Ghasemi, B. Aghabarari, M. Alizadeh, *et al.*, High efficiency decolorization of wastewater by Fenton catalyst: Magnetic iron–copper hybrid oxides, *J. Water Proc. Eng.*, 2020, **37**, 101540.
21 S. Yildiz and A. Olabi, Effect of Fe^{2+} and Fe^{0} Applied Photo-Fenton Processes on Sludge Disintegration, *Chem. Eng. Technol.*, 2020, **44**(1), 95–103.
22 Z. Izghri, G. Enaime, M. Eouarrat, *et al.*, Hydroxide Sludge/Hydrochar-Fe Composite Catalysts for Photo-Fenton Degradation of Dyes, *J. Chem.*, 2021, **2021**, 1–12.
23 G. Subramanian and H. Prakash, Photo Augmented Copper-based Fenton Disinfection under Visible LED Light and Natural Sunlight Irradiation, *Water Res.*, 2021, **190**, 116719.
24 J. Ji, R. M. Aleisa, H. Duan, *et al.*, Metallic Active Sites on MoO_2(110) Surface to Catalyze Advanced Oxidation Processes for Efficient Pollutant Removal, *iScience*, 2020, **23**(2), 100861.
25 C. M. Van Genuchten and J. Pena, Mn(II) Oxidation in Fenton and Fenton Type Systems: Identification of Reaction Efficiency and Reaction Products, *Environ. Sci. Technol.*, 2017, **51**(5), 2982–2991.
26 N. Xu, D. Guo and C. Xiao, Fe/Mn oxide decorated polyacrylonitrile hollow fiber membrane as heterogeneous Fenton reactor for methylene blue decolorization, *J. Appl. Polym. Sci.*, 2019, **136**(46), 48217.
27 K. K. Hazarika, H. Talukdar, P. Sudarsanam, *et al.*, Highly dispersed Mn_2O_3–Co_3O_4 nanostructures on carbon matrix as heterogeneous Fenton-like catalyst, *Appl. Organomet. Chem.*, 2020, **34**(4), e5512.

28 H. Liu, T. Xu, C. Li, *et al.*, High increase in biodegradability of coking wastewater enhanced by Mn ore tailings in Fenton/O_3 combined processes, *Int. J. Environ. Sci. Technol.*, 2020, **18**(1), 173–184.

29 A. Šuligoj, A. Ristić, G. Dražić, *et al.*, Bimetal Cu–Mn porous silica-supported catalyst for Fenton-like degradation of organic dyes in wastewater at neutral pH, *Catal. Today*, 2020, **358**, 270–277.

30 R. Zhang, L. Chen, B. Qiu, *et al.*, Biochar Derived from Treated Lotus Stem and Adsorption of Phthalic Acid Esters, *Water, Air, Soil Pollut.*, 2021, **232**(6), 1–12.

31 W. Huang, M. Zhang, Y. Wang, *et al.*, Biochars prepared from rabbit manure for the adsorption of rhodamine B and Congo red: characterisation, kinetics, isotherms and thermodynamic studies, *Water Sci. Technol.*, 2020, **81**(3), 436–444.

32 Z. Yang, X. Liu, M. Zhang, *et al.*, Effect of temperature and duration of pyrolysis on spent tea leaves biochar: physiochemical properties and Cd(II) adsorption capacity, *Water Sci. Technol.*, 2020, **81**(12), 2533–2544.

33 L. Lin, Z. Song, Y. Huang, *et al.*, Removal and Oxidation of Arsenic from Aqueous Solution by Biochar Impregnated with Fe–Mn Oxides, *Water, Air, Soil Pollut.*, 2019, **230**(5), 1–13.

34 X. Li and Y. Li, Adsorptive Removal of Dyes from Aqueous Solution by $KMnO_4$-Modified Rice Husk and Rice Straw, *J. Chem.*, 2019, **2019**, 1–9.

35 X. Zhang, Z. A. Ma, Z. Song, *et al.*, Role of Cryptomelane in Surface-Adsorbed Oxygen and Mn Chemical Valence in MnO_x during the Catalytic Oxidation of Toluene, *J. Phys. Chem. C*, 2019, **123**(28), 17255–17264.

36 Q. Zhao, Q. Liu, C. Song, *et al.*, Enhanced catalytic performance for VOCs oxidation on the CoAlO oxides by $KMnO_4$ doped on facile synthesis, *Chemosphere*, 2019, **218**, 895–906.

37 Z. Xiao, L. Zhang, L. Wu, *et al.*, Adsorptive removal of Cu(II) from aqueous solutions using a novel macroporous bead adsorbent based on poly(vinyl alcohol)/sodium alginate/$KMnO_4$ modified biochar, *J. Taiwan Inst. Chem. Eng.*, 2019, **102**, 110–117.

38 H. Shin, D. Tiwari and D.-J. Kim, Phosphate adsorption/desorption kinetics and P bioavailability of Mg-biochar from ground coffee waste, *J. Water Proc. Eng.*, 2020, **37**, 101484.

39 S. Kang, X. Li, J. Fan, *et al.*, Characterization of Hydrochars Produced by Hydrothermal Carbonization of Lignin, Cellulose, D-Xylose, and Wood Meal, *Ind. Eng. Chem. Res.*, 2012, **51**(26), 9023–9031.

40 M. C. Wang, G. D. Sheng and Y. P. Qiu, A novel manganese-oxide/biochar composite for efficient removal of lead(II) from aqueous solutions, *Int. J. Environ. Sci. Technol.*, 2014, **12**(5), 1719–1726.

41 V. Subramanian, H. Zhu, R. Vajtai, *et al.*, Hydrothermal Synthesis and Pseudocapacitance Properties of MnO_2 Nanostructures, *J. Phys. Chem. B*, 2005, **109**(43), 20207–20214.

42 M. Toupin, T. Brousse and D. Belanger, Charge storage mechanism of MnO_2 electrode used in aqueous electrochemical capacitor, *Chem. Mater.*, 2004, **16**(16), 3184–3190.

43 M. S. Kolathodi, S. N. Hanumantha Rao, T. S. Natarajan, *et al.*, Beaded manganese oxide (Mn_2O_3) nanofibers: preparation and application for capacitive energy storage, *J. Mater. Chem. A*, 2016, **4**(20), 7883–7891.

44 M. Chigane and M. Ishikaawa, Manganese oxide thin film preparation by potentiostatic electrolyses and electrochromism, *J. Electrochem. Soc.*, 2000, **147**(6), 2246.

45 M. Toupin, T. Brousse and D. Belanger, Influence of Microstructure on the Charge Storage Properties of Chemically Synthesized Manganese Dioxide, *Chem. Mater.*, 2002, **14**(9), 3946–3952.

46 S. Saha and A. Pal, Microporous assembly of MnO_2 nanosheets for malachite green degradation, *Sep. Purif. Technol.*, 2014, **134**, 26–36.

47 S. Paul, H. Kauser, M. S. Jain, *et al.*, Biogenic stabilization and heavy metal immobilization during vermicomposting of vegetable waste with biochar amendment, *J. Hazard. Mater.*, 2020, **390**, 121366.

48 X. Xiao, B. Chen and L. Zhu, Transformation, morphology, and dissolution of silicon and carbon in rice straw-derived biochars under different pyrolytic temperatures, *Environ. Sci. Technol.*, 2014, **48**(6), 3411–3419.

49 A. Naga Babu, D. Srinivasa Reddy, G. Suresh Kumar, *et al.*, Sequential synergetic sorption analysis of Gracilaria Rhodophyta biochar toward aluminum and fluoride: A statistical optimization approach, *Water Environ. Res.*, 2020, **92**(6), 880–898.

50 Z. Chen, B. Chen and C. T. Chiou, Fast and slow rates of naphthalene sorption to biochars produced at different temperatures, *Environ. Sci. Technol.*, 2012, **46**(20), 11104–11111.

51 H. Wang, Z. Huang, Z. Jiang, *et al.*, Trifunctional C@MnO Catalyst for Enhanced Stable Simultaneously Catalytic Removal of Formaldehyde and Ozone, *ACS Catal.*, 2018, **8**(4), 3164–3180.

52 J. Xu, J. Liu, P. Ling, *et al.*, Raman spectroscopy of biochar from the pyrolysis of three typical Chinese biomasses: A novel method for rapidly evaluating the biochar property, *Energy*, 2020, **202**, 117644.

53 A. Tagliaferro, M. Rovere, E. Padovano, *et al.*, Introducing the Novel Mixed Gaussian–Lorentzian Lineshape in the Analysis of the Raman Signal of Biochar, *Nanomaterials*, 2020, **10**(9), 1748.

54 Z. Sun, C. K. Russell and M. Fan, Effect of calcium ferrites on carbon dioxide gasification reactivity and kinetics of pine wood derived char, *Renewable Energy*, 2021, **163**, 445–452.

55 M. Giorcelli, P. Savi, A. Khan, *et al.*, Analysis of biochar with different pyrolysis temperatures used as filler in epoxy resin composites, *Biomass Bioenergy*, 2019, **122**, 466–471.

56 J. Inoue, A. Yoshie, T. Tanaka, *et al.*, Disappearance and alteration process of charcoal fragments in cumulative soils studied using Raman spectroscopy, *Geoderma*, 2017, **285**, 164–172.

57 Q. Cao, C. Chen, K. Li, *et al.*, Arsenic(v) removal behavior of schwertmannite synthesized by $KMnO_4$ rapid oxidation with high adsorption capacity and Fe utilization, *Chemosphere*, 2021, **264**(1), 128398.